

layers showed spin lifetimes of 1.6 ns at 275 K and equilibrium electron concentrations as low as  $5 \times 10^{16} \text{ cm}^{-3}$  (17), suggesting that the room-temperature spin precession that we observed is a general feature of *n*-doped semiconductors. In fact, these bulk samples exhibited an even weaker temperature dependence than seen in the QW structures, with the spin lifetime decreasing only 20% from 5 to 300 K. Interestingly, for undoped samples, elevation of the temperature increased  $T_2^*$  more than 10-fold above its low-temperature value, perhaps because of the thermal excitation of carriers or the thermal unbinding of excitons. For example, the precession lifetime at 2 T in the insulating QW (sample D) increased dramatically for temperatures above 80 K, rising from  $\sim 10$  ps at 5 K to  $\sim 0.2$  ns at 240 K. Similar behavior was seen in undoped ZnSe, where  $T_2^*$  was only a few picoseconds at 4 K but increased to 0.3 ns at 270 K.

We have demonstrated an optically active solid-state system in which electron spin polarization persisted for nanoseconds at room temperature. It appears that a primary function of the electron gas is to sweep holes out of the system, terminating the highly efficient electron-hole spin scattering. The Kerr effect is an essential tool for viewing this process, as the phenomenon occurs for electrons above  $E_F$  and is invisible to measures of spin relaxation such as the Hanle effect or time-resolved PL, which probe electrons near zero momentum. This technique allows us to witness spin lifetimes that far exceed the carrier recombination time and draws an interesting contrast to systems in which carrier recombination depletes the spin polarization an order of magnitude faster than spin relaxation processes (13, 18). We anticipate further insights into these spin relaxation processes with the extension of the time-resolved Kerr rotation technique to doped III-V semiconductors where both the elastic and inelastic scattering times are typically two orders of magnitude greater than in the samples studied here.

Although the observed precession reveals a memory of the initial spin orientation within the electronic system, its relation to individual spin coherence is not clear. Although electron-electron spin interactions of the form  $\mathbf{s}_i \cdot \mathbf{s}_j$  can destroy the coherence of individual spins with their initial orientation established by the optical field, they would have no impact on the measured Kerr signal because they do not alter the equations of motion for total electronic spin. These "hidden" decoherences rely on the absence of any spatial dependence to the spin interaction that would then couple to the orbital degrees of freedom, permitting spin relaxation. Because we cannot rule out such hid-

den processes, only a direct interference experiment (3, 4) can reveal the duration of quantum coherence within the spin precession. What we demonstrate here is that the contribution to spin decoherence from all other sources is quite small, even at room temperature. If these systems do prove to be quantum coherent for nanoseconds at room temperature, the development of ultrafast optical techniques to coherently manipulate the spin system would offer new technological opportunities.

#### REFERENCES AND NOTES

1. D. P. DiVincenzo, *Science* **270**, 255 (1995).
2. N. A. Gershenfeld and I. L. Chuang, *ibid.* **275**, 350 (1997).
3. S. Bar-Ad, I. Bar-Joseph, Y. Levinson, H. Shtrikman, *Phys. Rev. Lett.* **72**, 776 (1994).
4. A. P. Heberle, J. J. Baumberg, K. Kohler, *ibid.* **75**, 2598 (1995).
5. S. A. Crooker, J. J. Baumberg, F. Flack, N. Samarth, D. D. Awschalom, *ibid.* **77**, 2814 (1996).
6. \_\_\_\_\_, *Phys. Rev. B*, in press.
7. I. P. Smorchkova, N. Samarth, J. M. Kikkawa, D. D. Awschalom, *Phys. Rev. Lett.* **78**, 3571 (1997).

8. E. Burstein, *Phys. Rev.* **93**, 623 (1954).
9. G. Livescu *et al.*, *IEEE J. Quantum Electron.* **24**, 1677 (1988).
10. S. A. Crooker, F. D. Betz, J. Levy, D. D. Awschalom, *Rev. Sci. Instrum.* **67**, 2068 (1996).
11. G. L. Bir, A. G. Aronov, G. E. Pikus, *Zh. Eksp. Teor. Fiz.* **69**, 1382 (1975) [*Sov. Phys. JETP* **42**, 705 (1976)].
12. T. C. Damen, L. Vina, J. E. Cunningham, J. Shah, L. J. Sham, *Phys. Rev. Lett.* **67**, 3432 (1991).
13. J. Wagner, H. Schneider, D. Richards, A. Fischer, K. Ploog, *Phys. Rev. B* **47**, 4786 (1993).
14. F. Meier and B. P. Zakharchenya, Eds., *Optical Orientation* (North-Holland, Amsterdam, Netherlands, 1984).
15. R. J. Elliot, *Phys. Rev.* **96**, 266 (1954); F. Beuneu and P. Monod, *Phys. Rev. B* **18**, 2422 (1978).
16. M. I. D'yakanov and V. I. Perel', *Zh. Eksp. Teor. Fiz.* **60**, 1954 (1971) [*Sov. Phys. JETP* **33**, 1053 (1971)].
17. J. M. Kikkawa, I. P. Smorchkova, N. Samarth, D. D. Awschalom, unpublished results.
18. Ph. Roussignol *et al.*, *Phys. Rev. B* **46**, 7292 (1992); I. V. Kukushkin and V. B. Timofeev, *Adv. Phys.* **45**, 147 (1996).
19. Supported by grants from the Office of Naval Research (ONR N00014-97-1-0575 and N00014-97-1-0577) and the NSF Science and Technology Center for Quantized Electronic Structures (DMR 91-20007).

28 May 1997; accepted 10 July 1997

## Synthesis of Gallium Nitride Nanorods Through a Carbon Nanotube–Confined Reaction

Weiqliang Han, Shoushan Fan,\* Qunqing Li, Yongdan Hu

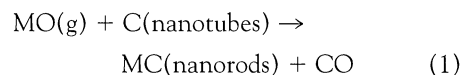
Gallium nitride nanorods were prepared through a carbon nanotube–confined reaction.  $\text{Ga}_2\text{O}$  vapor was reacted with  $\text{NH}_3$  gas in the presence of carbon nanotubes to form wurtzite gallium nitride nanorods. The nanorods have a diameter of 4 to 50 nanometers and a length of up to 25 micrometers. It is proposed that the carbon nanotube acts as a template to confine the reaction, which results in the gallium nitride nanorods having a diameter similar to that of the original nanotubes. The results suggest that it might be possible to synthesize other nitride nanorods through similar carbon nanotube–confined reactions.

The fabrication of nanometer-sized materials has gained considerable attention because of their potential uses in both mesoscopic research and the development of nanodevices. Here, we demonstrate the synthesis of crystalline GaN nanorods (nanowires) based on the recently discovered carbon nanotubes (1). GaN has promising applications for blue and ultraviolet optoelectronic devices and has attracted much attention recently after the successful fabrication of high-efficiency blue light-emitting diodes (2). Several approaches have been developed for synthesizing nanocrystalline GaN powder (3). To our knowledge, the synthesis of GaN nanorods (or nanowires) has not been reported to date.

Department of Physics and Center of Atomic and Molecular Sciences, Tsinghua University, Beijing 100084, China.

\*To whom correspondence should be addressed. E-mail: fss-dmp@mail.tsinghua.edu.cn

Recently, Dai *et al.* (4) reported an approach to the synthesis of nanoscale structures based on carbon nanotubes, in which the nanotubes were converted into carbide (MC) nanorods by reaction with a volatile oxide species. The reaction used was expressed as



where MO is a volatile metal or nonmetal oxide with a relatively high vapor pressure at the desired reaction temperature. Further studies on the formation of the carbide nanorods have suggested that the very stable carbon nanotube might act as a template, spatially confining the reaction to the nanotube, which results in the formation of nanorods (5, 6). We speculated that the method used to prepare carbide nanorods could be exploited to prepare

**Fig. 1.** Schematic diagram of the setup for preparing the GaN nanorods.

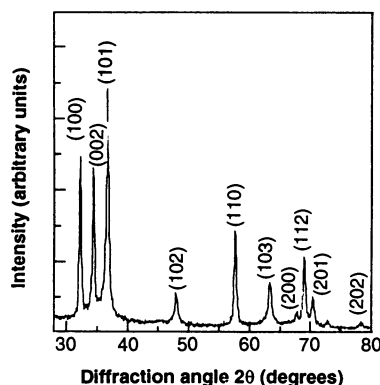
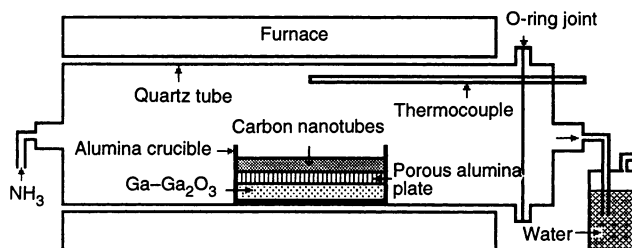
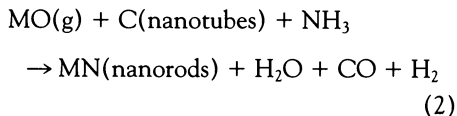


**Fig. 2.** XRD pattern of wurtzite GaN nanorods.

nitride (MN) nanorods through the reaction of carbon nanotubes with an MO in an ammonia atmosphere. The reaction can be expressed as



For the synthesis of crystalline GaN nanorods through reaction 2,  $\text{Ga}_2\text{O}$  was chosen as the MO. A Ga- $\text{Ga}_2\text{O}_3$  powder mixture was used as the starting material for  $\text{Ga}_2\text{O}$ . The  $\text{Ga}_2\text{O}$  vapor pressure over this mixture is about 1 torr at 1173 K (7). Carbon nanotubes were produced by metal-catalyzed decomposition of ethylene and hydrogen in a chemical vapor deposition system (8). The catalytic growth procedure yielded relatively pure multishell carbon nanotubes with typical diameters of around 15 nm. The reaction can be expressed as

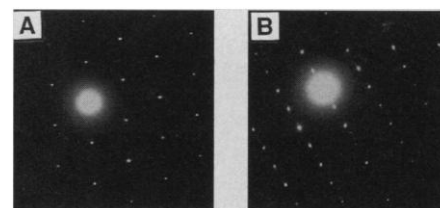
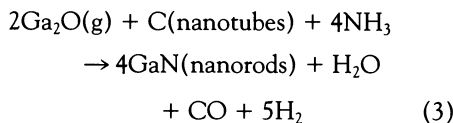


**Fig. 4.** Selected area of electron diffraction patterns of a wurtzite GaN nanorod. (A) The [001] diffraction pattern of the nanorod. (B) The [100] diffraction pattern of the nanorod.



Reaction 3 was carried out in a conventional furnace with a horizontal quartz tube. A 4:1 molar mixture of Ga and  $\text{Ga}_2\text{O}_3$  was placed in an alumina crucible and covered with a porous alumina plate with 3- to 5- $\mu\text{m}$  diameter channels. The carbon nanotubes were placed on the porous alumina plate. The crucible was placed in the hot zone inside the quartz tube (Fig. 1) and was held in a flowing ammonia atmosphere (400 standard cubic centimeters per minute) at 1173 K for 1 hour. It is expected that  $\text{Ga}_2\text{O}$  gas generated from the Ga- $\text{Ga}_2\text{O}_3$  powder mixture would flow toward the region of carbon nanotubes through the porous plate and react with the nanotubes and the  $\text{NH}_3$  gas.

After recovering the crucible from the furnace, we found that the original black carbon nanotubes on the porous alumina plate had turned into a layer of wool-like products of a light color. This layer of prod-

**Fig. 3.** (A) TEM image of the carbon nanotubes used as starting material. (B) TEM image of the GaN nanorods that were produced.

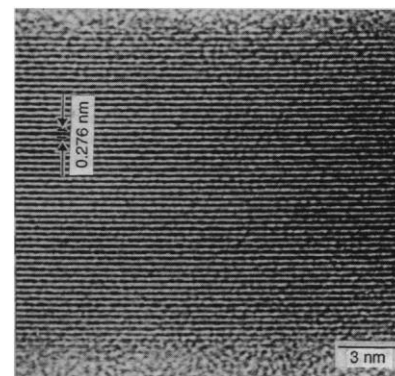
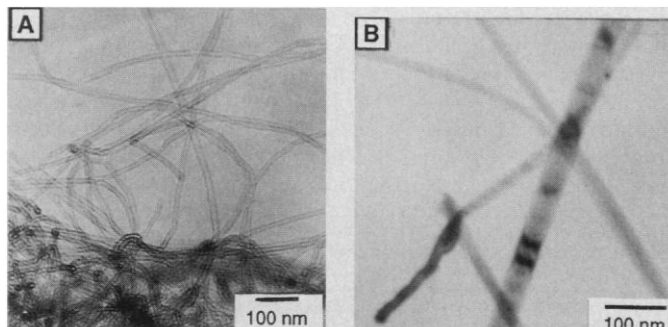


**Fig. 5.** HREM image of a 14.9-nm-diameter GaN nanorod whose (100) fringes are parallel to the edge of the nanorod.

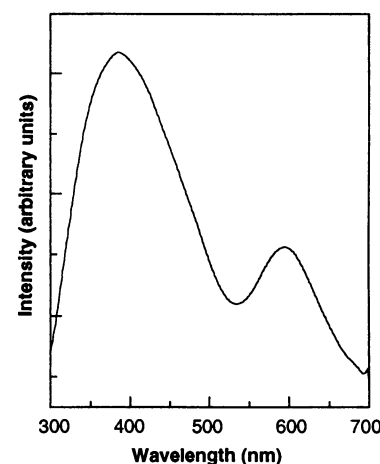


**Fig. 6.** PL spectrum of GaN nanorods.

ucts was characterized with a Rigaku (Tokyo, Japan) Dmax rB x-ray diffractometer with  $\text{Cu K}\alpha$  radiation ( $\lambda = 1.54178 \text{ \AA}$ ). In the x-ray diffraction (XRD) pattern (Fig. 2), the reflections can be indexed to hexagonal wurtzite GaN that has lattice constants  $a = 3.18 \text{ \AA}$  and  $c = 5.18 \text{ \AA}$ .

Transmission electron microscopy (TEM) images were taken with a Hitachi (Tokyo, Japan) H-800 transmission electron microscope. The TEM images showed that the products are relatively straight nanorods with diameters ranging from 4 to 50 nm, which are slightly different from the diameters of the starting nanotubes (Fig. 3) (9). The lengths of the nanorods are up to 25  $\mu\text{m}$ . The GaN nanorods are solid in contrast to the hollow core structure of carbon nanotubes. Selected area electron diffraction patterns (Fig. 4), taken from a single nanorod, are consistent with the single crystalline nature of the sample. The patterns can be indexed to the reflection of wurtzite GaN[001] (Fig. 4A) and GaN[100] (Fig. 4B). High-resolution transmission electron microscopy (HREM) images of GaN nanorods were taken on a Hitachi-9000NAR

transmission electron microscope. In the HREM image of a GaN nanorod with a diameter of about 14.9 nm (Fig. 5), the (100) fringes with the spacing of 0.276 nm are parallel to the edge of the nanorod.

In previous studies, GaN was prepared through the reaction  $\text{Ga}_2\text{O} + 2\text{NH}_3 \rightarrow 2\text{GaN} + \text{H}_2\text{O} + 2\text{H}_2$ ; however, the products were GaN powders (10). This reaction was also conducted at 1173 K for 1 hour in our experimental setup. There were no nanorod products observed under TEM. Also, a reaction of carbon nanotubes and  $\text{NH}_3$  was conducted at identical condition, which showed that the carbon nanotubes did not change in the absence of the Ga-Ga<sub>2</sub>O mixture. These experimental results provide further support for the idea that the GaN nanorod products formed on the porous alumina plate through reaction 3.

Photoluminescence (PL) spectra of the GaN nanorods were measured in a Perkin-Elmer (Buckinghamshire, UK) LS50B fluorescence spectrophotometer with a Xe lamp at room temperature under 254-nm ultraviolet light excitation. The filter wavelength was 290 nm. The PL spectrum (Fig. 6) consists of one strong broad emission peak at 384 nm and another emission peak at 595 nm, which is similar to the PL spectra of GaN reported previously (11).

We also prepared Si<sub>3</sub>N<sub>4</sub> nanorods using reaction 2 (12). The successful preparation of these nitride nanorods suggests that the method described in this report could be used to prepare a range of chemically distinct nitride nanorods, which might offer opportunities for both fundamental research and technological applications.

## REFERENCES AND NOTES

1. S. Iijima, *Nature* **354**, 56 (1991).
2. S. Nakamura, M. Senoh, T. Mukai, *Appl. Phys. Lett.* **62**, 2390 (1993); S. N. Mohammad, A. Salvador, H. Morkoc, *Proc. IEEE* **83**, 1306 (1995).
3. Y. Xie, Y. Qian, W. Wang, S. Zhang, Y. Zhang, *Science* **272**, 1926 (1996); K. E. Gansalvaes, G. Carlson, S. P. Rangarajan, M. Benaissa, M. Joseyacamman, *J. Mater. Chem.* **6**, 1451 (1996); H. Yamane, M. Shimada, S. J. Clarke, F. J. Disalvo, *Chem. Mater.* **9**, 413 (1997).
4. H. Dai, E. W. Wong, Y. Z. Lu, S. Fan, C. Lieber, *Nature* **375**, 769 (1995).
5. W. Wong, B. W. Maynor, L. D. Burns, C. M. Lieber, *Chem. Mater.* **8**, 2041 (1996).
6. W. Han *et al.*, *Chem. Phys. Lett.* **265**, 374 (1997).
7. C. J. Froesch and C. D. Thurmond, *J. Phys. Chem.* **66**, 877 (1962).
8. Q. Li, S. Fan, W. Han, C. Sun, W. Liang, *Jpn. J. Appl. Phys. Part 2* **36**, L501 (1997).
9. The spread of diameters of the nanorods prepared on the basis of the carbon nanotubes has also been observed in preparing SiC nanorods [see (6)], where a simple model has been suggested to explain this phenomenon. The model may also be helpful in explaining the spread of diameters of the GaN nanorods.
10. C. M. Balkas and R. E. Davis, *J. Am. Ceram. Soc.* **79**, 2309 (1996).
11. T. Ogino and M. Aoki, *Jpn. J. Appl. Phys.* **19**, 2395 (1980); T. Atuki *et al.*, *Appl. Phys. Lett.* **67**, 2188

- (1995); A. Argoitia *et al.*, *ibid.* **70**, 179 (1997).
12. Si<sub>3</sub>N<sub>4</sub> nanorods were prepared through the reaction of carbon nanotubes with SiO under nitrogen (or ammonia) atmosphere at 1673 K for 1 hour. The reaction scheme can be expressed as  $3\text{SiO}(g) + 3\text{C}(s) + 2\text{N}_2(g) \rightarrow \text{Si}_3\text{N}_4(s) + 3\text{CO}(g)$ . The nanorods

were 4 to 40 nm in diameter and up to 50 μm in length.

13. This work was supported by the Chinese National Foundation of Nature Science Research.

22 May 1997; accepted 14 July 1997

# Corona Formation and Heat Loss on Venus by Coupled Upwelling and Delamination

Suzanne E. Smrekar\* and Ellen R. Stofan

Coronae are volcanotectonic features that are unique to Venus and are interpreted to be small-scale upwellings. A model in which upwelling causes delamination at the edge of the plume head, along with deformation of a preexisting depleted mantle layer, produced the full range of topographic forms of coronae. If half of the coronae are active, delamination of the lower lithosphere could account for about 10 percent of Venus' heat loss, with another 15 percent due to upwelling. Delamination may occur in other geologic environments and could account for some of Venus' heat loss "deficit."

Venus is expected to be as geologically active as Earth because its size, mean density, and radioactive content indicate a comparable heat budget (1). The large and even distribution of unmodified impact craters suggests that Venus was geologically active until about 500 million years ago when activity apparently slowed (2). Critical questions for the evolution of Venus are what caused the decline in activity, how is Venus losing its heat, and why have Venus and Earth evolved so differently.

The tectonic style of a planet is defined by the mechanisms through which the hot, convecting interior, or mantle, transfers heat through the cold, stiff outer layer, called the thermal lithosphere. There are three geologically conventional end member methods of heat loss: hot spot volcanism, plate recycling (or plate tectonics), and lithospheric conduction (1). Hot spots, or surface manifestations of large-scale upwelling mantle plumes with broad (1000 to 2500 km) topographic rises, contribute only a small fraction (<5%) of Venus' heat budget (3). Data from the Magellan mission showed no evidence of global systems of spreading ridges, transform faults, and trenches that characterize terrestrial plate tectonics (4). Models of episodic heat loss (5), proposed to explain the apparent dearth of recent geologic activity, indicate that conduction through the lithosphere may currently be the dominant mechanism, but they do not actually predict the geologic signature of global overturn for comparison with observations. The thick litho-

sphere predicted by these models appears to be inconsistent with even a low level of ongoing volcanism and tectonism. The formation of coronae is consistent with a relatively thin lithosphere and may account for a significant portion of Venus' heat loss through small-scale mantle upwelling and recycling of the lower lithosphere through delamination.

Coronae are nearly circular annuli of fractures and ridges (Fig. 1) that are interpreted as manifestations of small-scale mantle upwelling driven by thermal buoyancy (6–8). There are about 360 coronae on Venus, ranging in diameter from ~100 to 2600 km, with most in a diameter range of 200 to 400 km (7). Here we address many of the outstanding questions in the study of coronae, including why they are unique to Venus, how the full range of topographic profiles are produced, the relation between the topography and the annulus of fractures that characterize coronae, the subduction zone morphology found on the edges of some coronae (9), and the cause of their complex geologic history (7).

Initial studies of coronae from Magellan radar images defined five classes primarily on the basis of the shape of the annulus: concentric, asymmetric, multiple, radial/concentric, or concentric-double ring (6). The topographic shapes of the 360 coronae on Venus were classified into nine groups (7) (Table 1). Group 3 includes corona shapes such as an elevated rim surrounding a central dome (Fig. 1), two nested topographic rings, and partial annular rims with irregular interior topography.

Models of corona formation (10–14) predict a dome, plateau, or an elevated interior surrounded by a rim and an outer moat caused by relaxation of a plateau

Jet Propulsion Laboratory, California Institute of Technology, MS 183-501, 4800 Oak Grove Drive, Pasadena, CA 91109, USA.

\*To whom correspondence should be addressed.